JOURNAL OF SOLID STATE CHEMISTRY 93, 534–548 (1991)

On The Crystal Structures of $La_2Ti_2O_7$ and $La_5Ti_5O_{17}$: High-Resolution Electron Microscopy

TIM WILLIAMS

CSIRO Division of Materials Science and Technology, Locked Bag 33, Clayton, Victoria 3168, Australia

HELMUT SCHMALLE AND ARMIN RELLER

Institute for Inorganic Chemistry, University of Zürich, Winterhurerstrasse 190, 8057 Zürich, Switzerland

AND FRANK LICHTENBERG, DANIEL WIDMER, AND GEORG BEDNORZ

IBM Research Division, Zürich Research Laboratory, 8803 Rüschlikon, Switzerland

Received November 26, 1990; in revised form April 9, 1991

The structure of $La_5Ti_5O_{17}$ has been examined by high-resolution transmission electron microscopy combined with powder X-ray and thermogravimetric analysis. It comprises five $[TiO_6]$ octahedra-thick layers isomorphous with {1 0 0} slabs of the $LaTiO_3$ orthorhombic perovskite structure, bounded by crystallographic shear parallel with the perovskite [0 0 1] direction. La atoms occupy the distorted perovskitic *A* sites. The structure is derived from the homologous $La_2Ti_2O_7$ by elimination of $\frac{1}{35}$ of the oxygens from this four-octahedra-thick layered structure. Both compounds are members of an homologous series based on variation in the anion to cation ratio.

1. Introduction

Two phases have been characterized in the $LaTiO_x$ system. In a quite recent study of $LnTiO_3$ perovskites grown from the melt the perovskite $LaTiO_3$ (with all Ti^{3+}) as well as the *Ln* = Nd, Sm, Gd, and Y titanates were shown to be orthorhombic rather than cubic (*1*). As in the $LnFeO_3$ (lanthanide orthoferrite) perovskites this difference from "ideal" cubic perovskite is due to distortion and tilting from the upright of the TiO_6 octahedral framework. $La_2Ti_2O_7$ was reported several years ago (*2, 3*) and the room temperature structure subsequently determined (*4, 5*). This structure (with fully oxidized Ti^{4+}) is not, however, that of cubic pyrochlore, which occurs for some of the "heavy rare-earth" plus transition metal oxides, but a layered structure comprising slabs of the $LaTiO_3$ perovskite four $[TiO_6]$ octahedra thick, bounded by shear on perovskitic {1 0 0} planes. The space group of this phase has been in contention [$P2_1$ (*4*) vs $Pna2_1$ (*5*)]; recently the results of a convergent-beam electron diffraction (CBED) study (*6*) suggested that the confusion over symmetry was due to microtwinning in one of the ear-

0022-4596/91 $3.00

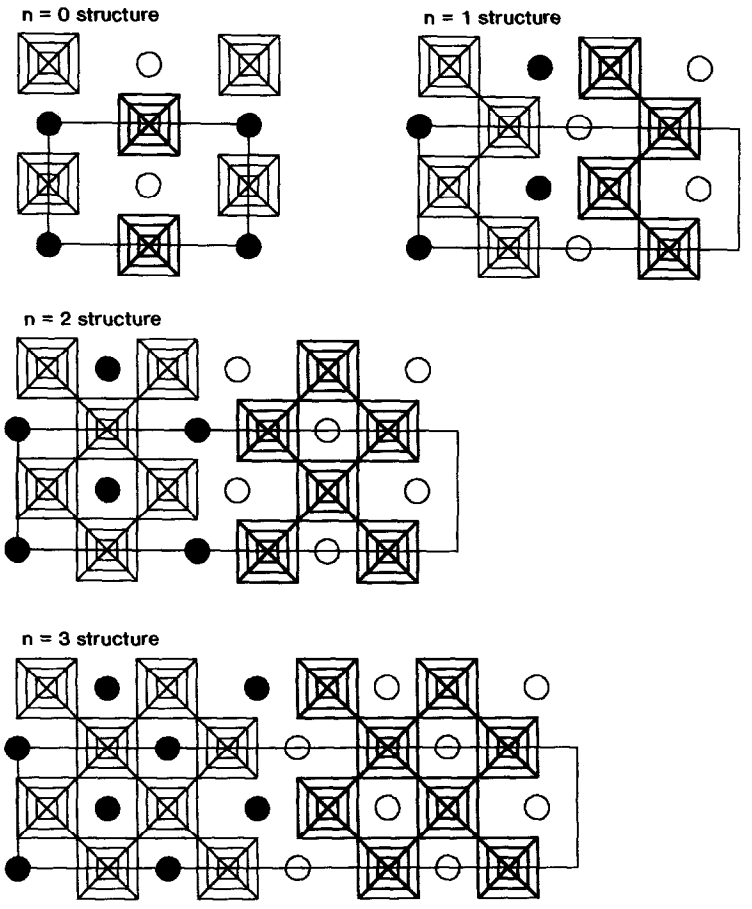

FIG. 1. The idealized structures of the first six members of the homologous series $A_{n+1}B_{n+1}O_{3n+5}$, $0 \leq n \leq 5$, shown in projection parallel with the ~3.9 (or ~7.8) Å repeat. Viewed parallel with a fourfold axis, B atoms occupy the centers and O atoms the vertices of the octahedra. Light and heavy ruling in the $[BO_6]$ octahedra indicates a height difference in the projection direction equal to half of one octahedron body diagonal, the B–O bond length of ~1.95 Å. Filled and open circles indicate La atoms also differing in height by this distance in adjacent slabs. Projected cells are ruled: these are single cells in the long (layering) direction for the two-layer thick orthorhombic forms of these structures, but double cells for, e.g., the monoclinic $n = 3$, 2-2-7 compound and other single-layer, $n = 2n + 1$ compounds with $\beta \neq 90°$.

lier samples, and showed that the correct space group for this phase at room temperature is $P2_1$, although an orthorhombic modification exists above 1053 K. This latter study also noted the existence of an incommensurate phase, stable between 993 K and the transition to orthorhombic symmetry. The structures of both twin individuals in a microtwinned crystal of $La_2Ti_2O_7$ grown by a floating-zone technique have been refined by us using X-ray methods and the results are reported elsewhere (7), showing that the twins are related by a mirror normal to c^*. The La–Ti cation sublattice is essentially undisturbed by the twinning, which results from two topologically identical choices of oxygen sublattice orientation.

$La_2Ti_2O_7$ (= $La_4Ti_4O_{14}$) is an $n = 3$ mem-

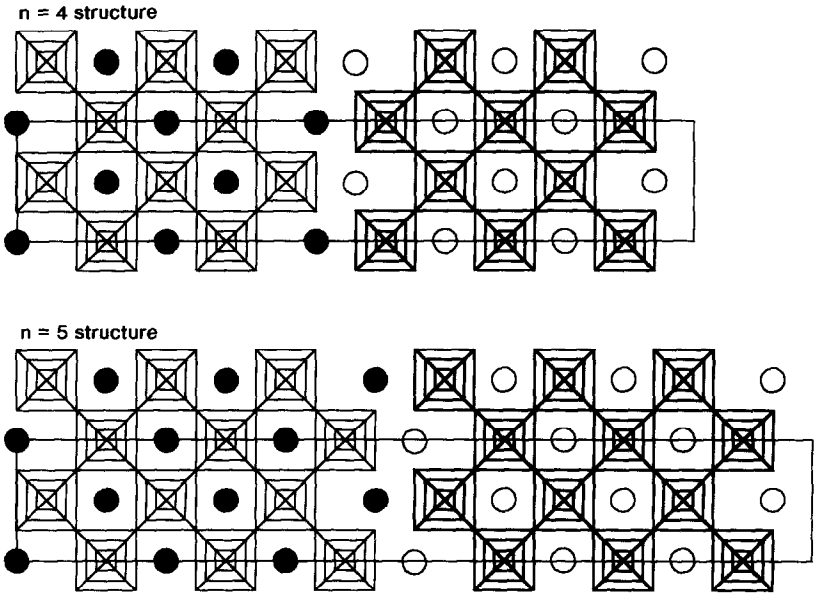

FIG. 1—*Continued*

ber of an homologous series of layered structures (*4, 8, 9*) $A_{n+1}B_{n+1}O_{3n+5}$, $0 \leq n \leq \infty$ (see Fig. 1), based on variation in the thickness of the component perovskitic slabs. The $n = 0$, ABX_5 and $n = 2$, $A_3B_3X_{11}$ members of the series are as yet unknown. The $n = 1$ members of this structural series are known only in the ABF_4 fluorides (typically, A = Ba, Sr; B = Mg, Mn, Fe, Co, Ni, Zn) (*10–12*) and the oxyfluoride $NaNbO_2F_2$ (*13*). An A-cation-deficient variant of this oxyfluoride structure exists in $Bi_4Nb_5O_{18}F$ (*14*), which can be described as $BiNb(O,F)_4$ with an additional row of $[NbO_6]$ octahedra in alternate layers. The $n = 3$ member is typified by monoclinic $La_2Ti_2O_7$ and $Ca_2Nb_2O_7$, and orthorhombic $Sr_2Nb_2O_7$ (*15*). Many other $n = 3$ compounds of titanates, niobates, and tantalates of the lanthanides and/or alkali metals are known, and some display piezo- and ferroelectricity. The compound $Sr_2Nb_2O_7$ has been studied extensively for both its ferroelectric properties [see, e.g., Nanamatsu, Kimura, and Kawamura (*16*)] and the incommensurate structure modulation (*17*). Higher n members exist in several quaternary systems: $n = 4$ and 5 in the Ca–Na–Nb–O (*8*) and La–Ca–Ti–O (*18*) systems, although they have not been reported in the ternaries and as yet the atomic positions of only the various $n = 1$ and 3 compounds have been determined accurately. Structures above $n = 5$ are only known as intergrowths from TEM studies. In Fig. 1, the idealized structures of the first six ($n = 0$ to 5) members of this family are illustrated. In Fig. 2, the topological ("orthorhombic") distortion of the perovskitic framework in these compounds is illustrated schematically for the $n = 3$ structure, in projection parallel with the ~5.5 Å axis common to all members of the family.

During a systematic synthetic and structural study of the $LaTiO_{3.5-x}$ system (*19*) and also quaternary and quinary systems containing additional B metals and with lanthanide (or lanthanide plus other large cation)-to-transition metal ratios ($A:B$) close to 1 : 1 (*20*), we prepared a new single phase

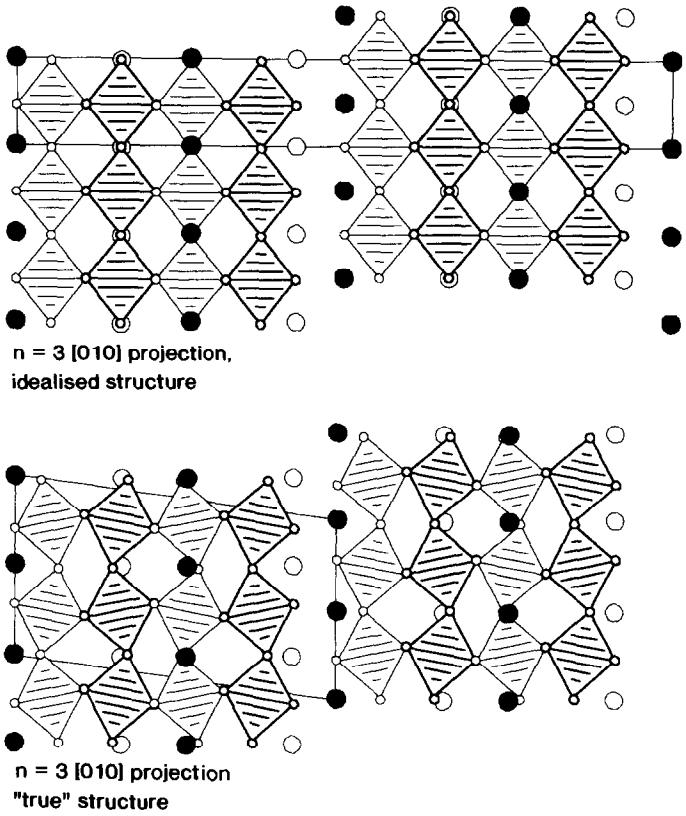

FIG. 2. Schematic illustration of the "orthorhombic distortion" of the $[BO_6]$ octahedral framework in 2-2-7. Upper diagram shows the perfect perovskitic array, approximately present in the compound $Sr_2Nb_2O_7$. In $La_2Ti_2O_7$, the framework is distorted, in common with the orthorhombic $LaTiO_3$ perovskite, and a monoclinic cell with a single-layer repeat is adopted (lower diagram). Large and small circles represent La and O atoms respectively; the filled La and heavily ruled octahedra lie at the same height in projection.

with the $n = 4$ layered structure. Here we describe the examination of the $n = 3$ and 4 La–Ti–O phases by high-resolution transmission electron microscopy (HRTEM) combined with powder X-ray diffraction (XRD) and thermogravimetry (TG). The $n = 3$, $La_2Ti_2O_7$ (referred to as "2-2-7" below), member is perfectly transparent and we were thus able to mechanically separate a (twinned, probably multiply so) "single" crystal fragment from the polycrystalline product rod by using optical microscopy, from which four-circle geometry single-crystal XRD data were collected and the positions of all atoms in both twin individuals refined unambiguously. The results of this study are reported in detail elsewhere (*7*). The structure of the second (new) phase discussed below, which is blue-black and opaque, was determined mainly from the HRTEM data supported by X-ray and TG measurements and is thus less accurate than that of the former structure. This material is referred to as 5-5-17 below, the lowest integral stoichiometry for $n = 4$, $La_5Ti_5O_{17}$. The results from quaternary lanthanum titanate systems containing also Sr and Nb will be reported in greater detail elsewhere (*20*).

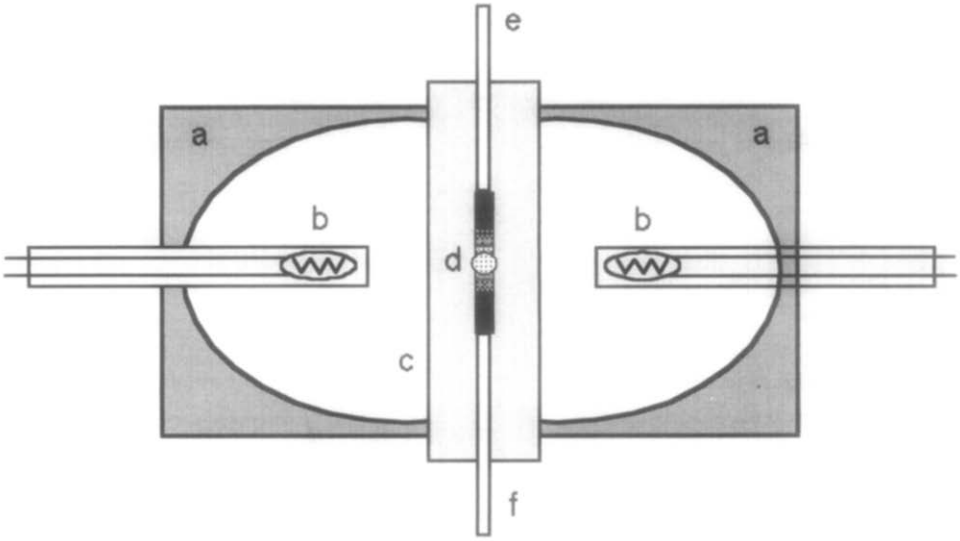

FIG. 3. Schematic illustration of the infrared zone-melting apparatus used to grow La–Ti–O compounds. (a) Internally gold-plated ovoid concave reflectors. (b) 1000-W quartz–halogen tungsten water- and air-cooled lamp located at one focus of each mirror. (c) Quartz work chamber. (d) Sample located at coincident foci of the reflector system. (e, f) Upper and lower specimen supports.

2. Experimental

2.1 Sample Preparation

The infrared floating-zone melting apparatus is shown schematically in Fig. 3. Except for the heat source, the method is similar to conventional radiofrequency (RF) floating-zone crystal growth of materials such as high-purity silicon. A "seed" crystal and polycrystalline ceramic "charge" rod are arranged coaxially at the coincident foci of two intersecting, ovoid mirrors. The mirrors are gold-coated on the highly polished interior surfaces to improve the reflectivity. At the second focus of each mirror a 1000-W quartz–halogen lamp is located. The lamps are both water- and air-cooled. Both the seed and the charge may be independently rotated about their long (vertical) axes and either raised or lowered, with vernier adjustments being provided for ensuring coaxiality of the rotation axes. The sample is isolated from the mirrors inside a quartz reaction tube, which can be evacuated prior to commencing a run and through which a variety of gases (O_2, N_2, Ar, and mixtures of the latter two with 4% H_2, etc.) may be passed at atmospheric pressure. Heating is controlled by varying the power applied to the lamps.

The ceramic charge materials were prepared from mixed high-purity oxides. By using an organic solvent or water to form the mixed powders into a stiff paste, rods were formed by pressing the paste into glass tubes of the appropriate diameter. These rods were pushed out, dried, and sintered overnight either in flowing argon or air at 1673 K. Usually, both seed and charge were of the same sintered ceramic material. The samples were then melted by passing the rods through the hot focus of the furnace at about 20 mm hr^{-1} while rotating the seed (the lower part) at a few tens of rpm. Due to the presence of visible light in the heat source, it was not possible to monitor the melt temperatures by optical pyrometry. The melting point of $LaTiO_3$ has previously been given as 2353 ± 20 K (*1*) and on the basis of the furnace power needed to melt

this phase (*19*) and also 2-2-7 and 5-5-17, the melting points appear to fall slightly with increasing oxygen content.

For both 2-2-7 and 5-5-17, the starting oxides were high-purity La_2O_3 and TiO_2. The former sample was sintered in air at 1673 K and then melted in flowing air. The latter was melted in a reducing N_2 + 4% H_2 mixture. 5-5-17 was also prepared from appropriate mixtures of La_2O_3 and TiO_2 + TiO, and sintered and melted under Ar with comparable results.

2.2 Powder X-Ray Analysis

As-grown 5-5-17 was examined in a Siemens D 500 diffractometer using Cu$K\alpha_1$ radiation. The powder diffraction data were used to refine the unit-cell by conventional least-squares methods, and to facilitate unambiguous indexing of the powder pattern, a pattern was simulated from the HRTEM structure using all atom positions in a cell halved in the **a** direction (discussed below), with the program LAZY-PULVERIX (*21*).

2.3 Thermogravimetric Analysis

The oxygen content of the reduced 5-5-17 sample was determined by reoxidizing in air at up to 1223 K in a Perkin–Elmer series TGS 7 thermal analysis system; these products were also subsequently characterized by TEM. A heating rate of 10 K min^{-1} was used with sample weights in the range 15–50 mg.

2.4 Transmission Electron Microscopy

TEM samples were prepared by crushing small pieces of the as-grown materials in ethanol in an agate mortar and placing a drop of the resulting suspension onto holey-carbon-coated copper support grids. Some support grids coated with gold were employed to internally calibrate the microscope camera constants. Three microscopes were used in this study: the E.T.H. Zürich PHILIPS CM 30 analytical microscope, a standard high-resolution 200-kV JEOL 200 CX machine at the University of Zürich, and the University of Cambridge 200-kV HREM, a specially modified JEOL 200 CX. The relevant parameters of the three machines are listed in Table I. Unless specifically noted, the imaging results considered below are from the CM 30. Images were generally recorded at optimum defocus from the extreme edges of suitable crystals.

TABLE I

PARAMETERS OF TRANSMISSION ELECTRON MICROSCOPES

200 kV, λ = 0.0251 Å		300 kV, λ = 0.01969 Å
JEOL 200 CX	Cambridge HREM	Philips CM 30
C_s = 1.2 mm	C_s = 0.5 mm	C_s = 1.2 mm
d_{min} = 2.41 Å	d_{min} = 1.94 Å	d_{min} = 2.01 Å
"extended Scherzer focus" condition		
−672 Å	−434 Å	−595 Å

Note. C_s, spherical aberration coefficient of objective lens; d_{min}, interpretable point resolution, defined for the first zero-crossing in the contrast transfer function as: $d_{min} = 0.649\ C_s^{0.25}\lambda^{0.75}$ (at the "extended Scherzer focus" objective excitation).

2.5 HRTEM Image Simulation

HRTEM Image simulations were done by the usual multislice method, using versions of programs by Anstis (*22*). For brevity, only relevant images are reproduced here for comparison with experimental images. Although not shown, images were also calculated for $La_2Ti_2O_7$ (2-2-7). For 5-5-17, atomic coordinates were derived from measurement of the HRTEM images as described below (3.2).

3. Results and Discussion

3.1 Unit Cell Determination

Examination by electron diffraction and imaging preceded the detailed interpretation of the X-ray data. Electron diffraction spot

patterns from as-grown 2-2-7 and 5-5-17 are shown in Figs. 4a–4f. In general, we observed very few anomalous effects in the patterns, suggesting that crystallinity was always high and the defect density very low (see below). In the [0 1 0] zone patterns of 5-5-17, the twinning on the {0 0 1} plane noted before in 2-2-7 (*6, 7*) was quite commonly observed as may be seen in the corresponding diffraction pattern (Fig. 4f). The twins were invariably present in different volume fractions, with often only a small fraction of one type (a few layers) present. From the gold-calibrated spot patterns and subsequently refinement of the powder X-ray pattern by least-squares, the unit cell given in Table II was deduced for 5-5-17. Kinematic extinction conditions ($h\ 0\ l$, $l = 2n + 1$ reflections systematically absent) suggest either *Pc* or *P2/c* as possible space groups for 5-5-17. Both compounds display pronounced orthogonal subcells and have rather similar true cells: the short *a* and *b* parameters could not be distinguished for the two compounds by electron diffraction alone and the intensity distribution of the $h\ k\ 0$ reflections was nearly identical for both samples. In both materials it appeared likely, from consideration of the diffracted intensities (the relatively weak $h\ 0\ l, h = 2n + 1$ reflections) and the HRTEM images, that the extremely pronounced orthogonal subcells were determined mainly by the cation positions, with lower symmetry (the monoclinic true cells and the true *a* axis) resulting from the oxygen sublattice. The $h\ 0\ l, h = 2n + 1$ reflection rows from both samples also show the twinning effect noted above. This is discussed in more detail below with regard to the HRTEM images from this zone.

3.2 Structure Analysis

Using enlargements of suitable images in the [1 0 0] and [0 1 0] orientations, cation positions for 5-5-17 (as projected columns of atoms) were estimated to ±0.5 Å. As the images were not "processed" we were not able to determine the cation positions very accurately; however, comparison of the measurements of images from 2-2-7, which has a known structure, and those from the new phase 5-5-17, suggested that such measurements were sufficiently accurate to enable us to unambiguously specify the cation positions in our model. In the [1 0 0] zone axis images from very thin regions (Figs. 5a and b) and again by comparison with the known structure of 2-2-7 = $La_2Ti_2O_7$, large and small black dots were taken to be the positions of the La and Ti atoms respectively and this enabled us to draft a working structure model quite easily. As oxygen positions could not be determined from the images directly, sites appropriate for the observed cations were used, assuming nearly regular octahedral coordination of the Ti atoms. For this reason, the model unit cell used in both image and X-ray simulations is halved in the **a** direction, as we were unable to locate the true oxygen positions and thus the origin of the cell *a* axis doubling.

The different *c* repeat of the two compounds is clearly visible in both [1 0 0] and [0 1 0] zone-axis images such as those shown in Figs. 5 and 6. The main difference between the two structures is in the thicknesses of the respective layers. Assuming that simple perovskitic layers are present in both materials, in 2-2-7 they are four [TiO_6] octahedra thick and in 5-5-17, five [TiO_6] octahedra thick across the layers; in both materials the interlayer boundary is a perovskitic {1 0 0} plane. Careful examination of the [1 0 0] zone axis images showed that there is another structural difference in 5-5-17, as the perovskite-like layers are slightly canted, in different directions ([0 1 0] and [0 $\bar{1}$ 0]) in alternate layers. This feature is clearly visible in the images of Fig. 5b. The one extra [TiO_6] octahedron in the layers of 5-5-17 more than doubles the *c* repeat from that of 2-2-7, a consequence of the monoclinic symmetry of both struc-

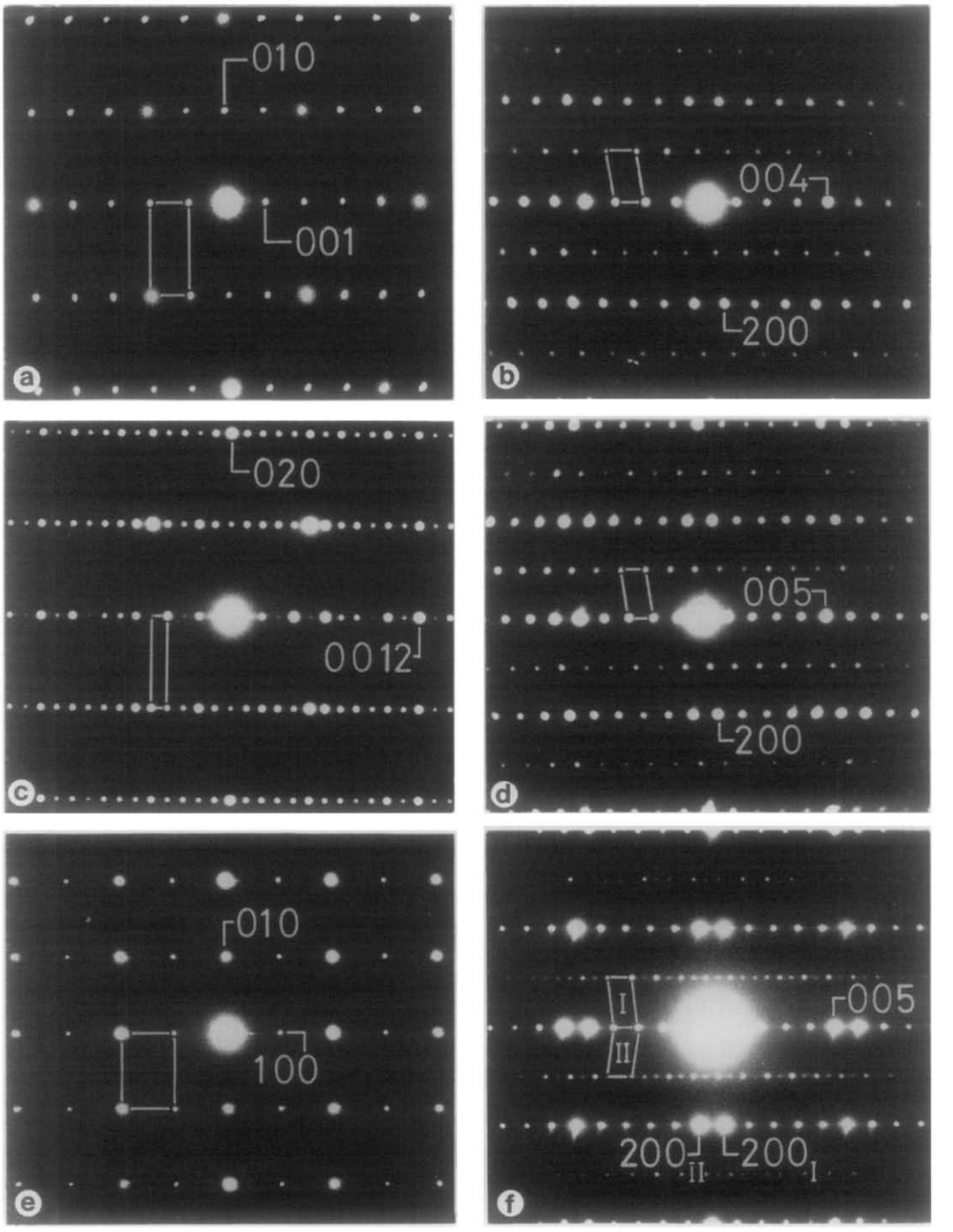

FIG. 4. Electron diffraction zone axis patterns (ZAP) for the main low-index zone axes of 2-2-7 and 5-5-17. Reciprocal cells are outlined for each pattern. (a, b) 2-2-7 ZAP from [1 0 0] and [0 1 0] zones, respectively; b is from an untwinned fragment (c, d) 5-5-17 ZAP, respectively, [1 0 0] and [0 1 0] with d from an untwinned fragment. (e) 5-5-17 [0 0 1] ZAP. (f) 5-5-17 [0 1 0] pattern from a twinned fragment; the two cells are outlined and the pattern shows the indexing for the two twins I and II.

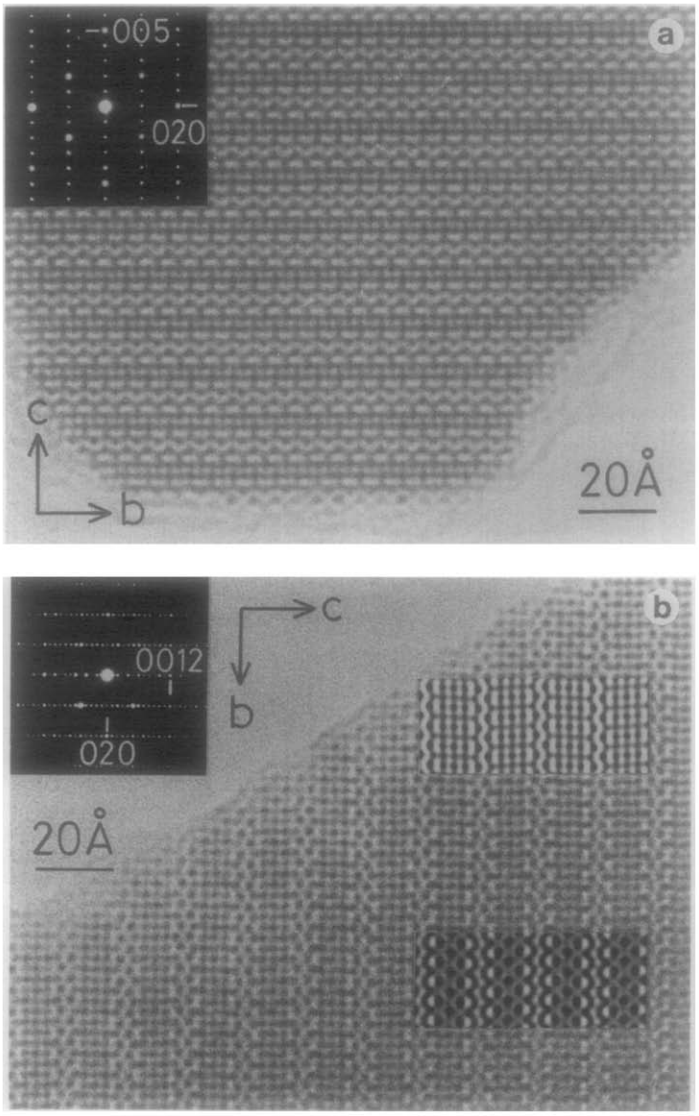

FIG. 5. [1 0 0] zone-axis HRTEM images from (a) 2-2-7 and (b) 5-5-17. The inset calculated images in b are for 23-Å (top) and 46-Å thick foils at −400 Å defocus. Both images were recorded at approximately the same defocus (Philips CM30).

tures. Whereas the orthorhombic $n = 3$ structures such as $Sr_2Nb_2O_7$ have two-layer cells, the monoclinic 2-2-7 has a single-layer thick cell, and the addition of one octahedron to both layers in 5-5-17 (as well as the layer canting) necessitates the double-layer cell repeat. With the same monoclinic angle (determined, as is the 7.9-Å cell a repeat by the orthorhombically distorted $[BO_6]$ octahedral framework: see Fig. 2), members of this homologous series with n = odd would thus have single-layer, and n = even, double-layer structures, all other parameters being equal.

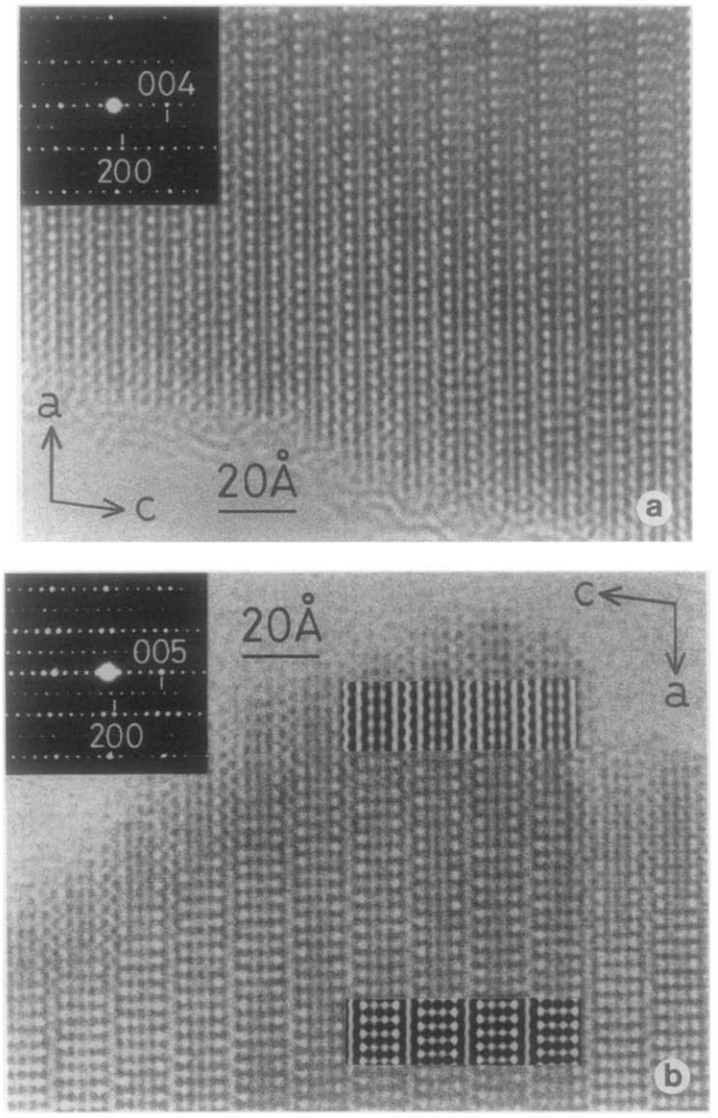

FIG. 6. [0 1 0] zone-axis HRTEM images from (a) 2-2-7 and (b) 5-5-17. The inset calculated images in b are for 22-Å (top) and 44-Å thick foils at −450 Å defocus. Again, both images were recorded at approximately the same defocus in the CM30, however, the image of b is of a crystal fragment lying over the carbon support grid and the contrast is therefore lower than in image a.

In the [0 1 0] zone-axis images of both materials (Fig. 6), there is less separation between atoms in projection and the images are thus less readily interpretable than in the [1 0 0] zone. However, the image contrast clearly supports the model of a layered structure for 5-5-17, and as can be seen both structures essentially comprise rather regular perovskite-like slabs, alternately sheared in the [1 0 0] direction up and down, by a distance of $\frac{1}{2}$ of a [TiO_6] octahedron long (four-fold) axis, i.e., one Ti–O bond length

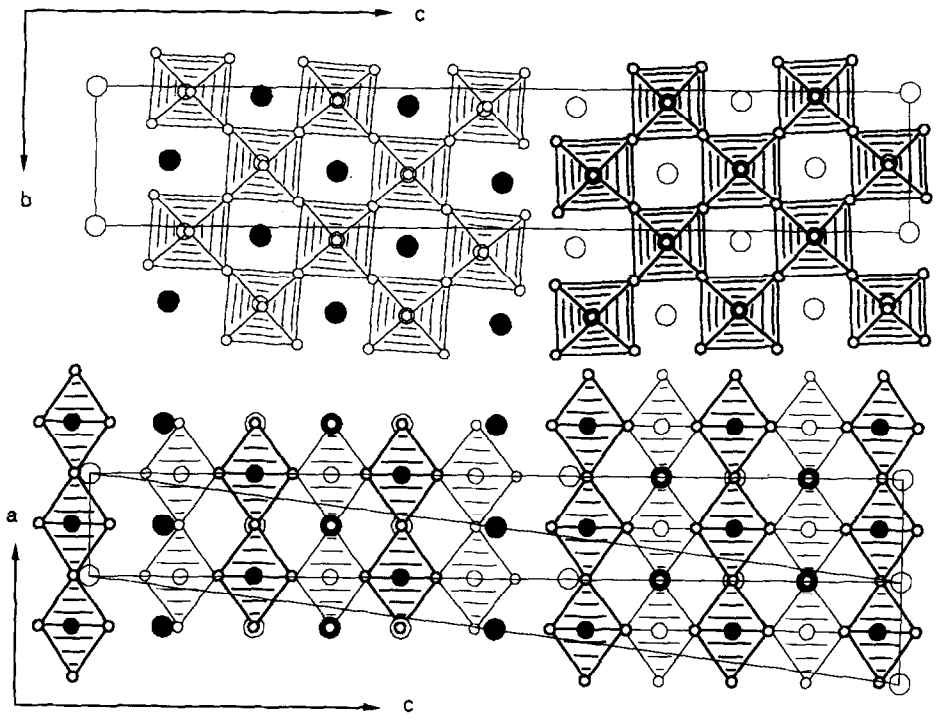

FIG. 7. The proposed half-*a* structure for 5-5-17 shown in the [1 0 0] and [0 1 0] projections. The unit cell outline in the [0 1 0] orientation (below) shows the orthogonal and monoclinic cell choices. Large, medium, and small circles represent La, Ti, and O atoms, respectively. La and Ti heights are suggested by open and closed circles and those of the octahedra by the light/heavy ruling.

($\approx$0.125 *a*). The layers comprise infinite slabs of [TiO_6] octahedra connected by sharing vertices and bounded by complex [LaO_x] polyhedra. In primitive cubic perovskite, the *A* cations are nominally 12-coordinated cuboctahedra, but in the orthorhombic perovskite $LaTiO_3$ and 2-2-7 the situation is one of more distorted, lower coordination *A* sites (*7*). These slabs, four [TiO_6] octahedra thick in 2-2-7 and five in 5-5-17, are relatively perfect in the center but the outermost boundary layers in both compounds are quite heavily distorted into zigzag rows as seen in the [1 0 0] images. The model structure deduced for 5-5-17 is shown in Fig. 7 in both the [1 0 0] and the [0 1 0] projections. The "canting" of the perovskitic slabs in the model is about 3°, or a shear of ~1 Å across one layer. This value was estimated from HRTEM images and might be expected to be somewhat inaccurate; however, it serves to illustrate the canting as a structural feature.

The cation stoichiometry of the 5-5-17 model was assumed to be the same as the starting materials, i.e., La/Ti = 1.0. The TEM images supply no information regarding this value and accurate energy-dispersive X-ray analysis in the CM30 TEM is problematical due to almost perfect overlap of La_L and Ti_K X-ray peaks. The model assumes full occupancy of all the [TiO_6] octahedron vertices by oxygens, thus giving $La_{10}Ti_{10}O_{34}$. Although the 2-2-7 phase cannot be reduced to any measurable weight loss even in flowing H_2 at 1000°C (*20*),

5-5-17, which was grown from the melt under 4% H_2 in N_2, oxidizes readily in O_2 or air at below 1000°C, thus we were able to confirm uptake of oxygen by 5-5-17 corresponding to the following reaction:

black, semiconducting 5-5-17 →

yellow, transparent insulator 2-2-7

$$2\ \text{“}La_5Ti_5O_{17}\text{”} + \tfrac{1}{2}O_2 \rightarrow La_{10}Ti_{10}O_{35}.$$

Stoichiometry change observed by TGA:

$$LaTiO_{3.42} \rightarrow LaTiO_{3.5}.$$

The sample of 5-5-17 examined most extensively by HRTEM and for which the X-ray data in Table II are presented thus has a slightly oxygen-rich stoichiometry, although HRTEM examination of other samples with oxygen stoichiometries between $LaTiO_{3.42}$ and $LaTiO_{3.36}$ gave no evidence for changes in the structure or symmetry and thus the structure appears to tolerate a fairly wide range of composition. On the basis of the above observations, it is clear that 5-5-17 represents the next highest member $n = 4$ in the homologous series $A_{n+1}B_{n+1}O_{3n+5}$ from $n = 3$, 2-2-7, formed by the addition of one [TiO_6] octahedron to the perovskitic slab thickness, which in the process more than doubles the unit cell c axis from ~13 to ~32 Å.

In neither the 2-2-7 nor the 5-5-17 [0 1 0] HRTEM images from very thin (~20 Å) regions was there direct evidence to support the true a repeat ≈ 7.9 Å, as the apparent periodicity of the dark (cation) sites was always half this value; neither was the twinning observed at the thin edges of crystals. In the electron diffraction patterns also, the $h\ 0\ l, h = 2n$ reflections are particularly pronounced and as noted above, the 7.9 Å repeat as well as the characteristic twinning reflections appear only as weak $h\ 0\ l, h = 2n + 1$ reflections in both materials. However, HRTEM images from moderately thick crystals in the [0 1 0] and [0 0 1] (Fig. 8) orientations show a weak doubling (modula-

TABLE II

POWDER X-RAY DIFFRACTION PATTERN FOR $La_5Ti_5O_{17}$ INDEXED ACCORDING TO THE DETERMINED MODEL STRUCTURE, AND THE RESULTING UNIT CELL CONSTANTS REFINED WITH ALL OBSERVED REFLECTIONS. TGA DETERMINED OXYGEN STOICHIOMETRY IS $LaTiO_{3.42}$.

Line	h	k	l	$d_{calc.}$	$d_{obs.}$	$I_{calc.}$	$I_{obs.}$
1	0	0	2	15.610630	15.626460	15.1	3.0
2	0	0	4	7.805314	7.805529	2.9	4.9
3	0	1	1	5.447156	5.450207	0.4	1.5
4	0	0	6	5.203543	5.201385	3.5	7.3
5	0	1	3	4.884768	4.886120	0.1	1.6
6	0	1	4	4.513366	4.511894	3.2	1.7
7	0	1	5	4.140738	4.140777	44.0	36.6
8	1	0	0	3.897615	3.896449	10.6	13.0
9	0	1	6	3.790262	3.789276	3.1	2.1
10	0	1	7	3.472203	3.470870	0.9	1.4
11	1	0	4	3.325638	3.322633	2.7	0.6
12	1	1	−1	3.202809	3.204821	5.0	9.7
13	0	0	10	3.122126	3.121288	100.0	100.0[a]
14	1	1	2	3.061459	3.062761	4.2	1.6
15	1	1	−5	2.962651	2.962686	39.7	74.0
16	0	2	0	2.766001	2.765572	62.5	25.4
17	1	1	−7	2.727080	2.725977	45.4	39.2
18	0	2	3	2.673196	2.673125	0.1	1.9
19	1	0	−10	2.599595	2.599715	17.6	13.5
20	0	1	11	2.525311	2.524273	4.0	7.0
21	1	1	8	2.353677	2.354311	0.4	3.1
22	1	0	−12	2.300060	2.300127	15.9	4.3
23	1	−2	0	2.255707	2.254896	13.8	10.7
24	0	0	14	2.230090	2.229754	5.7	5.3
25	1	2	−5	2.172068	2.171587	0.8	2.3
26	1	1	−12	2.123805	2.124505	0.7	2.9
27	0	2	10	2.070369	2.070462	40.7	17.5
28	1	0	12	2.049444	2.048360	0.7	2.6
29	1	1	−13	2.019046	2.018109	6.1	9.1
30	2	0	−2	1.964056	1.964073	72.5	19.7
31	0	1	15	1.948090	1.949321	8.3	12.8
32	1	1	12	1.921801	1.921258	0.9	1.1
33	0	2	12	1.895131	1.893954	11.4	12.8
34	1	1	15	1.829811	1.830006	4.0	8.1
35	2	1	−7	1.774335	1.774499	5.2	4.8
36	0	1	17	1.743003	1.743247	0.7	4.0
37	1	0	16	1.663993	1.664642	6.8	18.9
38	1	3	−5	1.632249	1.632684	4.6	5.3
39	2	2	−2	1.601405	1.600490	13.2	7.3
40	1	−3	−7	1.589355	1.589662	6.2	5.3
41	0	1	19	1.575201	1.575362	4.1	2.7
42	0	0	20	1.561063	1.561164	5.2	1.4
43	1	1	−19	1.524965	1.524989	2.1	5.6
44	2	2	8	1.425124	1.425741	10.8	12.5
45	0	4	0	1.383001	1.382992	4.2	5.7
46	2	2	−14	1.363540	1.363729	3.1	5.2
47	0	0	24	1.300886	2.300728	4.1	4.7
47	0	4	9	1.284672	1.283524	2.6	1.7[b]
48	1	−3	15	1.268570	1.268524	2.6	2.9

Note. $\lambda = 1.5406$ Å (Cu$K\alpha_1$); $a = 3.928$ Å; $b = 5.532$ Å; $c = 31.466$ Å; $\beta = 97.14$; $z = 2$; $\rho_{calc} = 5.9\ g \cdot cm^{-3}$; $V = 678.45$ Å^3. The true cell has $a' = 2a = 7.856$ Å and $z = 4$.

[a] Most intense observed reflection, to which others were normalized.

[b] Reflection rejected during least-squares refinement.

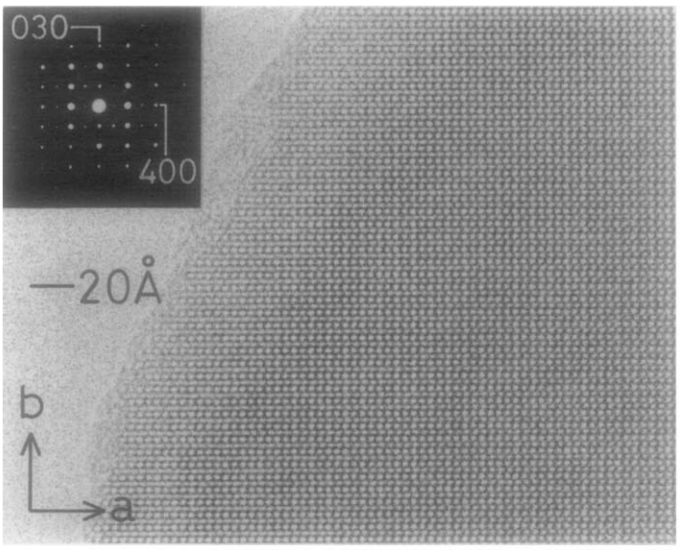

FIG. 8. HRTEM image from the [0 0 1] zone of 5-5-17. This image (200 CX) shows the true a repeat as indistinct vertical white lines, separated by two strong white dots (the a substructure repeat).

tion) of the $a/2$ period in the intensities of some rows of white spots. That the true a repeat can only be observed in images of thick regions where some appreciable dynamical scattering can occur suggests that this structural detail, as well as the twinning process, cannot be observed by kinematical diffraction as this is dominated by the cation substructure alone. As the microscopes we used were unable to resolve the oxygen positions directly (projected M–O distances are of the order of 1.5 ~ 2.0 Å; also the cation arrays scatter much more strongly than the oxygens), we were not able to determine the correct oxygen arrangement in either 2-2-7 or 5-5-17, but clearly some unobserved details of the anion lattice were contributing to the above observations. For this reason, obtaining high-quality single crystal X-ray data from both materials was of interest: this was not possible in the case of 5-5-17 as noted above but the structure of both twin individuals from the 2-2-7 sample could be refined. It was possible to confirm the structural origin of the twinning by combining the results of the HRTEM and single-crystal X-ray studies (*7*). In 2-2-7, the two twins are related by a mirror parallel with {001} and located midway between the shear planes. Slight canting of the [TiO_6] octahedra four-fold axes off [1 0 0], giving zig-zag columns of octahedra in the **a** direction (the orthorhombic distortion in the parent $LaTiO_3$ structure) results in the doubled a axis. Since both 2-2-7 and the perovskite end-member show this orthorhombic distortion it is probable that this, as well as doubling of a by the same process occurs in 5-5-17 too. This anion lattice distortion and also some small changes in the Ti–O bond lengths and La positions will probably account for the main differences between our model proposed here, effectively a one-half substructure, and an eventual full structural solution for this phase including the 7.8-Å a repeat.

4. Conclusions

On the basis of observations outlined above, it appears that in the ternary La $TiO_{3.5-x}$ system there exist at least two lay-

TABLE III

FRACTIONAL ATOMIC COORDINATES FOR ALL ATOMS IN PROPOSED STRUCTURE FOR $La_5Ti_5O_{17}$ (WITH CELL HALVED IN THE **a** DIRECTION, a = 3.928 Å)

Atom type	x/a	y/b	z/c
La	0.0	0.00	0.000
La	0.6	0.53	0.090
La	0.7	0.07	0.203
La	0.8	0.60	0.294
La	0.9	0.12	0.384
La	0.0	0.66	0.500
La	0.6	0.13	0.590
La	0.7	0.60	0.703
La	0.8	0.07	0.794
La	0.9	0.54	0.884
Ti	0.1	0.04	0.113
Ti	0.2	0.57	0.203
Ti	0.3	0.10	0.296
Ti	0.4	0.62	0.384
Ti	0.5	0.15	0.475
Ti	0.1	0.63	0.613
Ti	0.2	0.10	0.703
Ti	0.3	0.57	0.794
Ti	0.4	0.04	0.884
Ti	0.5	0.51	0.975
O	0.5	0.76	0.025
O	0.5	0.26	0.025
O	0.1	0.78	0.069
O	0.1	0.28	0.069
O	0.6	0.04	0.113
O	0.2	0.30	0.159
O	0.2	0.80	0.159
O	0.7	0.57	0.203
O	0.3	0.33	0.250
O	0.3	0.83	0.250
O	0.8	0.10	0.296
O	0.3	0.36	0.341
O	0.3	0.86	0.341
O	0.9	0.63	0.384
O	0.4	0.39	0.428
O	0.4	0.89	0.428
O	0.0	0.15	0.475
O	0.5	0.40	0.525
O	0.5	0.90	0.525
O	0.1	0.39	0.569
O	0.1	0.89	0.569
O	0.6	0.63	0.613
O	0.2	0.36	0.659
O	0.2	0.86	0.659
O	0.7	0.10	0.703
O	0.3	0.33	0.747
O	0.3	0.83	0.747
O	0.8	0.57	0.794
O	0.3	0.30	0.838
O	0.3	0.80	0.838
O	0.9	0.04	0.884
O	0.4	0.28	0.931
O	0.4	0.78	0.931
O	0.3	0.28	0.931
O	0.3	0.78	0.931

Note. Estimated errors in fractional atomic coordinates for all atoms are: $x/a \pm 0.1$ $y/b \pm 0.09$ $z/c \pm 0.015$, based on an estimated uncertainty in the measurement of HRTEM images of ~0.1 Å.

ered perovskite-related structures (in addition to the Ti^{3+} perovskite $LaTiO_3$) stable with different valencies of the Ti ions. For the newly characterized reduced phase $La_5Ti_5O_{17}$ a reasonably complete structural model for a cell halved in the **a** direction is proposed (Table III). We are currently studying this and related systems in order to elucidate the conditions necessary for synthesis both of possible higher members of the homologous series, i.e., structures between $n = 4$ $La_5Ti_5O_{17}$ and $n = \infty$ $LaTiO_3$ perovskite, and conversely of the first three structures (n = 0, 1, and 2 with B cation valencies greater than 4) and also for establishing routes to synthesis of these materials less extreme than employed in this work.

Acknowledgments

T.B.W. warmly thanks Professors H.R. Oswald, the University of Zürich, and G. Kostorz, E.T.H. Zürich, for their kind hospitality and provision of electron microscope time, and the Swiss National Foundation for Science for financial support under Project NF 2.772-0.87. We thank Stella Cassegrande and Barbara Heinz for help with TG measurements and Mark Fergus for photography. We are also very grateful to Dr. David Jefferson, Department of Physical Chemistry, the University of Cambridge, for providing time on the Cambridge 200 kV HREM and to Roland Wessiken and Peter Schwander, E.T.H. Zürich, for assistance with electron microscopy.

References

1. D. A. MACLEAN, H.-N. NG, AND J. E. GREEDAN, *J. Solid State Chem.* **30,** 35 (1979).

2. F. QUEYROUX, M. HUBER, AND R. COLLONGUES, *C.R. Acad. Sci. Paris C* **240,** 806 (1970).
3. J. K. BRANDON AND H. D. MEGAW, *Philos. Mag.* **21,** 189 (1970).
4. M. GASPERIN, *Acta Crystallogr. Sect. B* **31,** 2129 (1975).
5. K. SCHEUNEMANN AND H-K. MÜLLER-BUSCHBAUM, *J. Inorg. Nucl. Chem.* **37,** 1897 (1975).
6. M. TANAKA, H. SEKII, AND K. OHI, *Jap. J. Appl. Phys.* **24** suppl. 24-2, 814 (1985).
7. H. W. SCHMALLE, T. B. WILLIAMS, A. RELLER, AND J. G. BEDNORZ, submitted for publication.
8. R. PORTIER, M. FAYARD, A. CARPY, AND J. GALY, *Mater. Res. Bull.* **9,** 371 (1974).
9. R. J. D. TILLEY, *in* "Chemical Physics of Solids and their Surfaces" (M. W. Roberts and J. M. Thomas, Eds.), Ch. 6, p. 121, Royal Society of Chemistry, Great Britain (1980).
10. M. EIBSCHÜTZ AND H. J. GUGGENHEIM, *Solid State Commun.* **6,** 737 (1968).
11. H. G. VON SCHNERING AND P. BLECKMANN, *Naturwissenschaften* **55**(7), 342 (1968).
12. E. T. KEVE, S. C. ABRAHAMS, AND J. L. BERNSTEIN, *J. Chem. Phys.* **51,** 4928 (1969).
13. S. ANDERSSON AND J. GALY, *Acta Crystallogr. Sect. B* **25,** 847 (1969).
14. L. KIHLBORG, M. SUNDBERG, AND Ö. SÄVBORG, *Ultramicroscopy* **18,** 191 (1985).
15. N. ISHIZAWA, F. MARUMO, T. KAWAMURA, AND M. KIMURA, *Acta Crystallogr. Sect. B* **31,** 1912 (1975).
16. S. NANAMATSU, M. KIMURA, AND T. KAWAMURA, *J. Phys. Soc. Jpn.* **38,** 817 (1975).
17. N. YAMAMOTO, *Acta Crystallogr. Sect. A* **38,** 780 (1982).
18. M. NANOT, F. QUEYROUX, AND J.-C. GILLES, *C.R. Acad. Sci Paris. Ser. C* **277,** 505 (1973).
19. F. LICHTENBERG, D. WIDMER, G. BEDNORZ, T. WILLIAMS, AND A. RELLER, *Z. Phys. B.* **82,** 211 (1991).
20. T. B. WILLIAMS, F. LICHTENBERG, D. WIDMER, A. RELLER, AND J. G. BEDNORZ, in preparation.
21. K. YVON, O. DE FIORE, AND E. PARTHE, *J. Appl. Crystallogr.* **10,** 73 (1977).
22. ANSTIS, personal communication (1985).